

Synaptic inhibition and excitation estimated via the time constant of membrane potential fluctuations

Rune W. Berg and Susanne Ditlevsen

J Neurophysiol 110:1021-1034, 2013. First published 1 May 2013;
doi: 10.1152/jn.00006.2013

You might find this additional info useful...

This article cites 58 articles, 27 of which you can access for free at:
<http://jn.physiology.org/content/110/4/1021.full#ref-list-1>

Updated information and services including high resolution figures, can be found at:
<http://jn.physiology.org/content/110/4/1021.full>

Additional material and information about *Journal of Neurophysiology* can be found at:
<http://www.the-aps.org/publications/jn>

This information is current as of August 22, 2013.

Synaptic inhibition and excitation estimated via the time constant of membrane potential fluctuations

Rune W. Berg¹ and Susanne Ditlevsen²

¹Faculty of Health Sciences, Department of Neuroscience and Pharmacology, University of Copenhagen, Denmark;
and ²Department of Mathematical Sciences, University of Copenhagen, Denmark

Submitted 4 January 2013; accepted in final form 29 April 2013

Berg RW, Ditlevsen S. Synaptic inhibition and excitation estimated via the time constant of membrane potential fluctuations. *J Neurophysiol* 110: 1021–1034, 2013. First published May 1, 2013; doi:10.1152/jn.00006.2013.—When recording the membrane potential, V , of a neuron it is desirable to be able to extract the synaptic input. Critically, the synaptic input is stochastic and nonreproducible so one is therefore often restricted to single-trial data. Here, we introduce means of estimating the inhibition and excitation and their confidence limits from single sweep trials. The estimates are based on the mean membrane potential, \bar{V} , and the membrane time constant, τ . The time constant provides the total conductance ($G = \text{capacitance}/\tau$) and is extracted from the autocorrelation of V . The synaptic conductances can then be inferred from \bar{V} when approximating the neuron as a single compartment. We further employ a stochastic model to establish limits of confidence. The method is verified on models and experimental data, where the synaptic input is manipulated pharmacologically or estimated by an alternative method. The method gives best results if the synaptic input is large compared with other conductances, the intrinsic conductances have little or no time dependence or are comparably small, the ligand-gated kinetics is faster than the membrane time constant, and the majority of synaptic contacts are electrotonically close to soma (recording site). Although our data are in current clamp, the method also works in V -clamp recordings, with some minor adaptations. All custom made procedures are provided in Matlab.

fluctuations; balanced; inhibition; excitation; network; maximum likelihood estimation; membrane resistance; synaptic; conductance; Ornstein-Uhlenbeck process

AN INTRACELLULAR RECORDING of the neuronal membrane potential, V , reflects the synaptic input from the surrounding network. To investigate the neuronal function, it is desirable to be able to estimate incoming inhibition and excitation. When synaptic input is high rather than low it is easier to measure, and such a state is often referred to as *high-conductance state* (Destexhe et al. 2003). This state often has concurrent excitation and inhibition and thus has limited excursions in V . Numerous studies report such synaptic mixtures, referred to as *balanced excitation and inhibition* (E/I; Shadlen and Newsome 1994), especially in the cerebral cortex (Okun and Lampl 2008; Shu et al. 2003). It has been suggested that balanced E/I serves to increase responsiveness (van Vreeswijk and Sompolinsky 1996), e.g., to sensory input (Hasenstaub et al. 2007; Wehr and Zador 2003; Wilent and Contreras 2004). Concurrent E/I has also been found in the brainstem respiratory system (de Almeida and Kirkwood 2010; Parkis et al. 1999), spinal cord

(Berg et al. 2007), and in invertebrates (Sasaki et al. 2009; Baca et al. 2008). When the balance is perturbed or compromised, it often has severe consequences, e.g., epilepsy (Dichter and Ayala 1987; Cobos et al. 2005), schizophrenia (Kehrer et al. 2008), or Alzheimer's disease (Palop et al. 2006; Roberson et al. 2011). It is therefore important to gain knowledge of synaptic conductance dynamics and methods for doing so are in demand.

Previous methods have been suggested (Maltenfort et al. 2004), some which are based on the mean (Berg et al. 2007; Borg-Graham et al. 1998; Mariño et al. 2005; Monier et al. 2008) and variance of V (Rudolph et al. 2004). These estimates either have poor temporal resolution or require two or more different I - V measurements to dissect total conductance (G_{tot}) as the slope of the I - V plot. Unfortunately, this approach depends on precise trial-to-trial reproduction of the same state, which poses high requirements on data quality. If synaptic fluctuations are smaller than the trial-to-trial variability, the method comes short. Furthermore, estimates of conductance are greatly improved if these are high, since it warrants the neglect of other conductances. However, inadvertently, if inhibition and excitation are high, sensitivity to imbalances is also high, and the requirement of reproducibility becomes difficult.

Because of this caveat of trial-to-trial irregularity (Azouz and Gray 1999; Yarom and Hounsgaard 2011), it would be helpful to have a method where single-trial data are sufficient. Here, we introduce such a method based on extracting G_{tot} in an I - V -clamp recording via the membrane time constant, τ . The time constant is extracted in periods short enough to assume stationarity yet large enough to establish statistics. First, the autocorrelation function of V will decay with τ assuming stationarity and monoexponential decay (Fig. 1). Second, we use the analytically tractability of a stochastic model to establish confidence limits (Bachar et al. 2013). We test the method on simulated data as well as real data from motoneurons in a functional spinal network. The estimates are compared with estimates using the traditional method of multitrial data and further verified by reducing synaptic conductance via pharmacological manipulation.

MATERIALS AND METHODS

A neuron, which reliably can be characterized as a single electrical compartment, has a voltage dynamics across the membrane that is given by the differential equation

Address for reprint requests and other correspondence: R. W. Berg, Dept. of neuroscience and pharmacology, Univ. of Copenhagen, Blegdamsvej 3, DK-2200 Denmark (e-mail: runeb@sund.ku.dk).

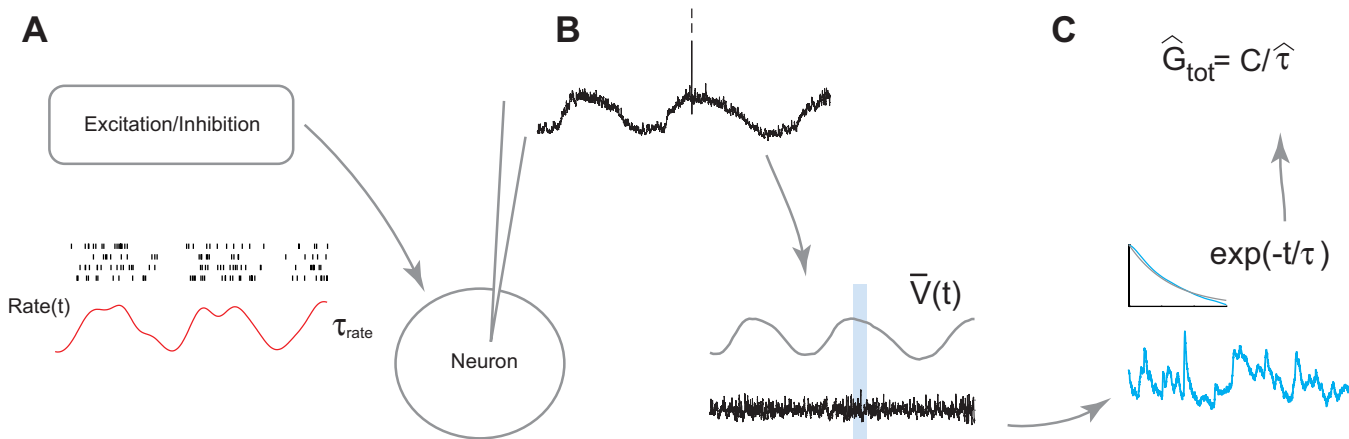


Fig. 1. Illustration of method of extraction of the time-dependent mean membrane conductance and mean membrane potential. *A*: presynaptic neurons project to the neuron with a rate intensity that varies on a slow timescale compared with the rate itself ($\tau_{\text{rate}} \gg \tau$). *B*: membrane potential of the neuron is recorded with prominent synaptic fluctuations. V is now divided into a slow and a fast varying part. Taking a small time window, the slow part represents \bar{V} , whereas the fast part represents the synaptic fluctuations. *C*: autocorrelation function of the fluctuations decays at a rate given by τ , which is extracted and the inverse gives total conductance (G_{tot}).

$$\begin{aligned} C \frac{dV}{dt} &= -G_L(V - E_L) - G_e(V - E_e) - G_i(V - E_i) + I_{\text{inj}} + \eta(t) \\ &= -G_{\text{tot}}(V - E_{\text{tot}}) + I_{\text{inj}} + \eta(t) \quad (I) \end{aligned}$$

where C is the total capacitance, G_L , G_e , and G_i are the leak, excitation, and inhibition conductances; E_L , E_e , and E_i are their respective reversal potentials; and $\eta(t)$ is a zero mean noise process taking into account the random arrivals of synaptic input. In current-clamp recordings, the injected current I_{inj} is known, since it is imposed by the experimenter. In voltage clamp, the clamped potential is known, and the necessary injected current to maintain this potential is measured. Regardless of the chosen method the equation ties V together with I_{inj} via the conductance. The total conductance is given by $G_{\text{tot}} = G_L + G_i + G_e$, and E_{tot} is the total weighted reversal potential for all the conductances, $E_{\text{tot}} = (G_L E_L + G_i E_i + G_e E_e)/G_{\text{tot}}$. Then, $\bar{V} = E_{\text{tot}} + I_{\text{inj}}/G_{\text{tot}}$ is the asymptotic mean of V . All reversal potentials and the leak conductance, G_L , are assumed constant in time. The membrane time constant is $\tau = C/G_{\text{tot}}$. Since the surface area, thickness, and dielectric constant of the cell membrane of the neuron are assumed constant, C is also constant.

Current vs. Voltage Clamp

The experimental measurements has to be performed as either current clamp, i.e., keeping the injected current constant, or voltage clamp where the current is adjusted to maintain constant membrane potential. In the present study we use current clamp, and therefore most of the analysis is adapted to this paradigm, but the equations and analysis can easily be adjusted to fit voltage clamp data, in the following way. In I -clamp recordings, τ is extracted from the fluctuations in V . In V -clamp recordings, τ is extracted from fluctuations in I . The rest of the analysis of estimating total conductance, excitation and inhibition, and their levels of confidence remains the same.

Estimating Inhibition and Excitation

Assume that for a given data window it is reasonable to consider V stationary, and thus, within the given window, G_{tot} and \bar{V} are constant. The data window size is discussed below. We can then estimate G_i and G_e reasoning as follows. Since V is stationary, on average the time derivative in Eq. 1 is zero, and taking expectations we obtain

$$-G_L(\bar{V} - E_L) - G_e(\bar{V} - E_e) - G_i(\bar{V} - E_i) + I_{\text{inj}} \approx 0 \quad (2)$$

where the mean membrane potential, \bar{V} , enters instead of V itself. In V clamp, we average I_{inj} and write \bar{I}_{inj} . Combining with the equation $G_{\text{tot}} = G_L + G_e + G_i$, we get the following expressions of the inhibitory and excitatory conductances,

$$G_e = G_{\text{tot}} - G_i - G_L \quad (3)$$

where G_i is given by

$$G_i = \frac{G_L(E_L - E_e) + G_{\text{tot}}(E_e - \bar{V}) + I_{\text{inj}}}{E_e - E_i}. \quad (4)$$

The constants G_L , E_e , E_i , and E_L are assumed known from prior experiments as explained below, and G_{tot} and V (or \bar{I}_{inj}) are estimated for the given window. Finally, by letting the window slide through the data trace, estimates of the time evolution of G_i and G_e are obtained.

We estimate G_{tot} and \bar{V} from I -clamp intracellular recordings. Suppose the membrane potential V is sampled at N time points with sampling step Δt and that in a given window, v_j is the j th sample point of V for $j = 0, 1, \dots, n$ with $n \ll N$. Then G_{tot} and \bar{V} are estimated from the sample $\{v_j\}_{j=0, \dots, n}$ as explained in the following paragraphs. In voltage clamp, it corresponds to the sampled i_j s.

Estimating the Total Conductance

G_{tot} is given as C/τ and τ can be estimated from the dynamics of V (or I_{inj}). This can be achieved by perturbing V by injecting brief current pulses and measure the decay back to E_{tot} . However, this gives discrete measurements, which may be undesirable if there is a time evolution in the input rate or the synaptic input itself contaminates the estimates. An alternative way of estimating τ is to directly utilize the V fluctuations caused by random arrival of synaptic input. If the change in synaptic input rate is slow compared with τ itself, τ can be estimated from the V recordings in a window, which is large compared with τ , but small compared with the rate of change in synaptic input rate (Fig. 1, *A* and *B*). The most direct and nonparametric estimation of τ is via the autocorrelation function (ACF) of V (Fig. 1*C*). For the leaky integrate-and-fire neuronal models with linear drift, the ACF has an exponential decay with time constant equal to τ (Forman and Sørensen 2008; Jahn et al. 2011). For more realistic models and experimental data, the ACF will not be exactly exponential, because of other underlying processes with different time constants, e.g., ligand-gated ion channel kinetics or low-pass filter properties of the membrane. Nevertheless, it is reasonable to assume the ACF positive and decreasing, and the exponential can serve as an approximation. Thus the rate of decay in the ACF of V offers a means to estimate G_{tot} .

G_{tot} from autocorrelation function. The ACF for a stationary process is defined as the covariance between two values of the process at different points in time divided by their variance, as function of the time lag between observations; $R(t) \equiv \text{Cov}[V(t+s), V(s)]/\text{Var}(V)$. By definition it takes values between -1 and 1 . As estimator, we use the sample autocorrelation function added a correction term to compensate for the negative bias (Kendall 1976),

$$\hat{R}_m = \hat{R}(m\Delta t) = \frac{\sum_{j=0}^{n-m} (v_j - \bar{v})(v_{j+m} - \bar{v})}{\sum_{j=0}^n (v_j - \bar{v})^2} + \frac{2m}{n} \quad (5)$$

where $m\Delta t$ is the time lag between observations, and $\bar{v} = \sum_{j=0}^n v_j / (n+1)$ is the average. Note that $\hat{R}(0) = 1 = R(0)$ always. We only use the estimates for $m \leq k$ for some $k \ll n$ because the estimates become increasingly unreliable for increasing m . In particular, we set $k = 30-40$ corresponding to 3–4 ms. We then make a linear regression of the logarithm of $\hat{R}_0, \hat{R}_1, \dots, \hat{R}_k$ on $0, \Delta t, \dots, k\Delta t$, thus obtaining an estimate of τ . Alternatively, a nonlinear regression can be performed on the original data. A few comments are in order. The usual estimate for $e^{-\Delta t/\tau}$ when assuming an exponential decay in the autocorrelation function is simply given by \hat{R}_1 , possibly without the correction term. Since we are using the exponential decay only as an approximation to a possibly more complex autocorrelation function, \hat{R}_1 will bias the result towards the shape of the autocorrelation of order one. We therefore include estimated autocorrelations of higher order as well to fit the exponential decay, such that misfits will be averaged out over longer lags. We also include the intercept as a free parameter in the regression, instead of fixing it to $\log(1) = 0$, letting the fitted curve be more flexible over a larger range. An approximation to the variance of \hat{R}_m is given by $[(1 - \rho^{2m})(1 + \rho^2)/(1 - \rho^2) - 2m\rho^{2m}]/n$, where $\rho = e^{-\Delta t/\tau}$ (Bartlett 1946). Note how it is increasing in m . The variance of \hat{G}_{tot} is given by the usual variance estimate of the slope parameter in a linear regression.

Maximum likelihood estimation of G_{tot} and \bar{V} . An alternative to the ACF method is to apply maximum likelihood estimation (MLE) of G_{tot} in an assumed stochastic model (Pospischil et al. 2009). Assuming that the noise term in Eq. 1 is Gaussian, we get the generic Ornstein-Uhlenbeck (OU) stochastic differential equation (Tuckwell 1988; Gerstner and Kistler 2002; Ditlevsen and Lansky 2005),

$$C \frac{dV(t)}{dt} = -G_{\text{tot}}[V(t) - \bar{V}] + \sigma \xi(t) \quad (6)$$

where σ is scaling the variance, and $\xi(t)$ is a Gaussian white noise process with zero mean and unit standard deviation. This description is a simplification of more biophysical realistic models like the Hodgkin-Huxley type models, which typically operate on multiple time scales. In the model (Eq. 6) the faster processes, like synaptic dynamics, have been averaged out. The important point is that the data will only be compatible with the model (Eq. 6) on time scales, which are long compared with the fast time scales of those processes that are not explicitly modeled, for example, the synaptic time constants appearing in Eq. 16 below. Subsampling of the data, at some rate to ensure that the data are analyzed on a scale where the model is appropriate, can be used to remove some of the problems arising from the intrinsic multiscale character of the data, like bias in the estimate of the total conductance (Pavlou and Stuart 2007). The range of time scales at which the OU process (Eq. 6) is approximately valid is unknown. However, this can be assessed empirically to some extent (see Figs. 3G and 7D). The MLEs of G_{tot} and \bar{V} with appropriate subsampling are given as solutions to the equations (Ditlevsen and Lansky 2012),

$$\hat{\bar{V}} = \frac{(v_n - v_0 e^{-\Delta/\hat{\tau}})}{n(1 - e^{-\Delta/\hat{\tau}})} + \frac{1}{n} \sum_{j=1}^{n-1} v_j \approx \frac{1}{n+1} \sum_{j=0}^n v_j = \bar{v} \quad (7)$$

$$\frac{\hat{G}_{\text{tot}}}{C} = \frac{1}{\hat{\tau}} = -\frac{1}{\Delta t} \log \left(\frac{\frac{1}{n-m+1} \sum_{j=m}^n (v_j - \hat{\bar{V}})(v_{j-m} - \hat{\bar{V}})}{\frac{1}{n} \sum_{j=1}^n (v_{j-1} - \hat{\bar{V}})^2} \right) \quad (8)$$

where the symbol $\hat{\cdot}$ indicates it is an estimator. Note the similarity between Eqs. 8 and 5. Here, m has to be chosen such that the subsampling is at an appropriate rate. The asymptotic variances of \hat{G}_{tot} and $\hat{\bar{V}}$ in Eq. 8 obtained by inverting the Fisher information are $\text{Var}[\hat{G}_{\text{tot}}] \xrightarrow{\text{as}} 2G_{\text{tot}}C/n\Delta t$ and $\text{Var}[\hat{\bar{V}}] \xrightarrow{\text{as}} \sigma^2/n\Delta t G_{\text{tot}}^2$.

There are some caveats that may contaminate the estimation of the time constant. For instance, since the estimators are based on models with no spiking mechanism included, and subthreshold oscillations of experimental data are conditioned on not crossing the spiking threshold, a bias is introduced in the estimates (Bibbona and Ditlevsen 2012). The problem is largest for fluctuations close to the threshold. Another caveat arises from bias caused by finite sample sizes. Especially the time constant is degraded when the length of the observation interval, $n\Delta t$, is not very large compared with τ (Ditlevsen and Lansky 2012).

Uncertainties in G_{tot}

The uncertainty in \hat{G}_{tot} can be approximated via the asymptotic variance of \hat{G}_{tot} given above. Thus the ~95% confidence limits for G_{tot} assuming an OU process are

$$\hat{G}_{\text{tot}} \pm 2\sqrt{2\hat{G}_{\text{tot}}C/n\Delta t}, \quad (9)$$

where $n\Delta t$ is the temporal size of the window.

Uncertainties in G_i and G_e

To assess the uncertainties in the estimated inhibitory and excitatory conductances, we use Eqs. 3 and 4, and the variances of the estimators of \bar{V} and G_{tot} , regardless of how we estimate G_{tot} . We obtain

$$\text{Var}[\hat{G}_i] \approx \frac{\text{Var}[\hat{G}_{\text{tot}}](E_e - \bar{V})^2 + G_{\text{tot}}^2 \text{Var}[\hat{\bar{V}}]}{(E_e - E_i)^2} \quad (10)$$

$$\text{Var}[\hat{G}_e] \approx \frac{\text{Var}[\hat{G}_{\text{tot}}](E_i - \bar{V})^2 + G_{\text{tot}}^2 \text{Var}[\hat{\bar{V}}]}{(E_e - E_i)^2} \quad (11)$$

where terms of order $1/(n\Delta t)^2$ are ignored. Note how the excitatory conductance is more accurately determined than the inhibitory conductance due to the larger driving force of excitatory input, since \bar{V} is much closer to E_e than E_i . Expressions in Eqs. 10 and 11 can then be used to construct approximate confidence limits for G_i and G_e by $\hat{G}_i \pm 2\sqrt{\text{Var}[\hat{G}_i]}$, where the estimates for G_{tot} and \bar{V} and their variances are inserted, and likewise for G_e . Note how Eqs. 9–11 also work for other methods of estimation of G_{tot} than via MLE.

Time-Independent Parameters

The leak conductance, G_L , total capacitance, C , and the reversal potentials for leak, inhibition and excitation, E_L , E_i , and E_e , are considered constant throughout the course of recording. Therefore, we can estimate these parameters during conditions where the synaptic inputs are small or absent. In that situation, G_{tot} is equal to the leak conductance, G_L , and the resting membrane potential is equal to E_L .

If these conditions are not present in the course of the experiment, for instance, if there is a substantial background synaptic activity, the leak conductance can be estimated via the principle that conductance is larger than or equal to zero. The total conductance, $G_{\text{tot}} = G_L + G_i + G_e$, is measured during steady and minimal synaptic input, thus assuming $G_{\text{tot}} \approx G_L$.

The inhibitory reversal potential can be measured by imposing a current ramp to vary V and observe where the inhibitory postsynaptic potentials (IPSPs) reverse. The point of reversal in potential is E_i by definition. This is possible when the spontaneous rate of input is low enough to allow identification of the IPSPs. If the IPSPs fuse together due to higher intensity input, assessing E_i becomes difficult. Nevertheless, a bias in E_i is reflected in the analysis, since a E_i with a positive bias would give rise to a negative G_i . Since conductance cannot be negative, the sign of G_i provides a means to verify the initial estimate of E_i . Estimating E_e is more difficult because it is often ~ 0 mV, far from the resting membrane potential, and shifting V to the point of excitatory postsynaptic potential (EPSP) reversal would require a large positive injected current. Such a large current would likely kill the cell. Nevertheless, due to the large driving force of excitatory input, a precise estimate of E_e is of minor importance (Eqs. 10 and 11).

The total capacitance, C , is determined by the membrane area and the thickness and dielectric constant of the lipid bilayer (Golowasch et al. 2009). For simplicity, we assume C constant throughout the recordings and associated with a proper compensation of electrode capacitance. Hence, C can be estimated during quiescent periods, as the product of time constant and G_L ($C = \tau G_L$), for instance, by giving brief current pulses and fitting an exponential decay to V .

Contribution from Voltage-Dependent Intrinsic Conductance

Thus far we have assumed all intrinsic conductances either zero or constant such that they can be included in G_L . In this way we are ignoring the contribution of voltage-sensitive conductances, such as persistent Na^+ , K^+ , and Ca^{2+} , which result in a nonlinear relation between current and V [for a review, see Russo and Hounsgaard (1999)]. Though this is likely to be a valid approximation in a high-conductance state (Alaburda et al. 2005; Destexhe et al. 2003) during intense synaptic input (Berg et al. 2008; Destexhe and Paré 1999) or in V -clamp recordings, it may be less valid during low-intensity input. The strongest subthreshold V -sensitive conductance is the Ca^{2+} current. The Na^+ and K^+ voltage-dependent currents are mainly responsible for the spiking mechanism, which are brief and can therefore often be ignored. Most of the conductances are activated for depolarization above -70 mV, but some are activated for hyperpolarizing potentials too, e.g., I_h current. One way to address the issue is to include the conductance in the calculation, assuming they are in steady state for the given V . When there is only one major contributor of intrinsic V -sensitive conductance that has no time dependence, the simplest approach is to include this conductance, denoted G_{int} , in Eq. 1

$$\frac{dV}{dt} = -G_{\text{syn}}(V - E_{\text{syn}}) - G_L(V - E_L) + I_{\text{inj}} - G_{\text{int}}(V)(V - E_{\text{int}}) \quad (12)$$

where $G_{\text{syn}}(V - E_{\text{syn}}) = G_e(V - E_e) + G_i(V - E_i)$. Then, $G_{\text{int}}(V)$ can be estimated in a similar way as G_L , while the synaptic input is either small or zero. Such situation can be before evoking a sensory input or after termination of the experiment with assistance of pharmacology to prevent synaptic input. In current clamp, the membrane potential is then recorded for different current injections, or vice versa in voltage clamp, to establish the I - V curve. The shape of the I - V curve is then fitted to a polynomial and the first derivative is an estimate of G_{tot} as a function of V . Since $G_{\text{syn}} \approx 0$, G_{int} is just the residual from $G_{\text{tot}} - G_L$. The synaptic conductance then has a V -dependent term added in Eqs. 3 and 4,

$$G_e = G_{\text{tot}} - G_i - G_L - G_{\text{int}}(\bar{V}) \quad (13)$$

where G_i is given by

$$G_i = \frac{G_L(E_L - E_e) + G_{\text{tot}}(E_e - \bar{V}) + I_{\text{inj}} + G_{\text{int}}(\bar{V})(E_{\text{int}} - E_e)}{E_e - E_i} \quad (14)$$

The assumption includes that the V -dependent conductance is independent of time and unaltered by the synaptic input, i.e., there is no neuromodulation. If there are a temporal dependence of a strong and slow intrinsic conductance or action potentials, the approach is less likely to succeed. Furthermore, if there are multiple major contributors of intrinsic conductance that cannot be ignored, the task is increasingly difficult and one has to estimate the conductance as a function of V for each, as well as their reversal potentials. This can most likely only be accomplished by assistance of pharmacology at the end of the experiment.

Ohmic Conductance: Multitrial Data

The assistance of multitrial data provides an independent means of estimating the membrane conductance. Under the assumption that the network state is reproducible, the synaptic input can be estimated by applying different current injections and carefully aligning the recorded membrane potential (see Fig. 6A). The slope of the I - V curve reveals the total conductance and the evolution provides the time dependence of G_{tot} (see Fig. 6B). We refer to this conductance as the *ohmic conductance* or the *ohmic method*. The inhibitory and excitatory conductances can be calculated using this estimate of G_{tot} and Eqs. 3 and 4 (see Fig. 6C). The estimates of G_e and G_i can be performed for each trial, i.e., each set of V and I_{inj} . We use this ohmic estimate of G_{tot} to verify the estimates using ACF.

Experimental Preparation

Integrated preparation. Red-eared turtles (*Trachemys scripta elegans*) were placed on crushed ice for 2 h to ensure hypothermic anesthesia. Animals were killed by decapitation and blood substituted by perfusion with a Ringer solution containing the following (mM): 120 NaCl, 5 KCl, 15 NaHCO_3 , 2 MgCl_2 , 3 CaCl_2 , and 20 glucose, saturated with 98% O_2 -2% CO_2 to obtain pH 7.6. The carapace containing the D4-D10 spinal cord segments was isolated by transverse cuts and removed from the animal, similar to studies published elsewhere (Alaburda and Hounsgaard 2003). The surgical procedures complied with Danish legislation and were approved by the controlling body under the Ministry of Justice.

Recordings. Approximately 40 intracellular recording trials in current-clamp mode (ranging from -2.5 to $+2.5$ nA) were performed with a Multiclamp 700B amplifier (Molecular Devices). The glass pipettes were filled with a mixture of 0.9 M potassium acetate and 0.1 M KCl. Intracellular recordings were obtained from neurons in segment D9/D10. Recordings were accepted if neurons had a stable V less than -50 mV. Data were sampled at 20 kHz ($\Delta t = 0.05$ ms) with a 12-bit analog-to-digital converter (Digidata 1440A from Molecular Devices), displayed by means of Axoscope and Clampex software. Hip flexor nerve activity was recorded with a differential amplifier Iso-DAM8 (World Precision Instruments) using a suction pipette. The bandwidth was 100 Hz to 1 kHz. Activation of scratch program in the network: tactile activation was performed with the fire-polished tip of a bent glass rod mounted to the membrane of a loudspeaker touching the skin. The duration, frequency, and amplitude of the stimulus were controlled with a function generator. The following drugs were used: In the first step, a glycinergic receptor antagonist was added to the superfusion solution (strychnine; 10 μM). In the second step, the glutamatergic receptor antagonist 6-cyano-7-nitroquinoxaline-2,3-dione (CNQX; 25 μM ; Tocris) was added to the superfuse solution.

Choice of Data Window Size

A data window in which it is reasonable to assume V stationary has to be chosen for the analysis. Since the distribution of V is constantly changing, stationarity has to be understood as the changes in distribution are slow compared with the length of the window. The presence of slow trends will bias the estimation of the autocorrelation, and we therefore recommend high-pass filtering of V such that any slow modulations are removed and the faster fluctuations that reveal τ remain. If the window is small, the variance of the estimators will be large, whereas if the window is large, the bias caused by nonstationarity will be large. Thus this is a typical bias-variance tradeoff, where we seek to minimize both errors due to bias and errors due to variance. Ideally, results will not depend too much on the specific choice of window size for some intermediate interval. We chose a window size of 130 ms in our simulations and 300 ms in the analysis of real data, which seemed to provide a good trade off between temporal resolution and high correlation with the ohmic estimate (see Fig. 7D). Principled methods to choose the optimal window size can be designed, e.g., Kobayashi et al. (2011) employed an empirical Bayes method to choose the relevant smoothing parameter; see also Hastie et al. (2008) for a general treatment.

Conductance-Based Model with Poisson Synaptic Input

We also test our method on simulated data from a single-compartment conductance-based integrate-and-fire model with synaptic inhibitory and excitatory input arriving at two Poisson rates, λ_i and λ_e (Kolind et al. 2012; Kuhn et al. 2004), which we refer to as the GPS model. The synaptic input generates a transient increase in the membrane conductance, which is selective to either Na^+ , i.e., excitatory or K^+/Cl^- , i.e., inhibitory conductance. The membrane potentials follow the equation:

$$\frac{dV}{dt} = -G_L(V - E_L) - \sum_j g_{e,j}(t)(V - E_e) - \sum_k g_{i,k}(t)(V - E_i) + I_{\text{inj}} \quad (15)$$

where $g_{e,j}(t)$ and $g_{i,k}(t)$ are the j th and k th excitatory and inhibitory post synaptic conductance, respectively. For each of the j th and k th input a transient conductance is elicited modeling the opening of a single postsynaptic contact as an α -function. The α -function is defined by

$$g_{\text{syn}}(t') = \frac{t'}{\tau_{\text{syn}}} g_{\max} e^{1 - \frac{t'}{\tau_{\text{syn}}}}, \quad t' > 0 \quad (16)$$

where g_{\max} is the maximal conductance, τ_{syn} is the characteristic time constant from a single postsynaptic input, and t' is the time after arrival of a single synaptic input. Both τ_{syn} and g_{\max} are different for inhibition and excitation, but otherwise constant for those inputs. Values used in the simulations are $\tau_{\text{syn},e} = 0.1$ ms and $g_{\max,e} = 17.8$ nS for excitation and $\tau_{\text{syn},i} = 0.5$ ms and $g_{\max,i} = 9.4$ nS for inhibition. The balance of \bar{V} is achieved by adjusting the mean inhibitory conductance once given an excitatory conductance according to the direct relation

$$\bar{g}_i = \frac{G_L(E_L - \bar{V}) + \bar{g}_e(E_e - \bar{V})}{\bar{V} - E_i} \quad (17)$$

The mean synaptic conductances are related to the Poisson input rates as $\lambda_e = \bar{g}_e/\tau_{\text{syn},e} g_{\max,e}$ and $\lambda_i = \bar{g}_i/\tau_{\text{syn},i} g_{\max,i}$ (Kolind et al. 2012), where e is the exponential number. Hence, the input in the model is varied by changing \bar{g}_e and calculating what the \bar{g}_i should be in the balanced condition and their corresponding Poisson rates of input, λ_i and λ_e . A capacitance of $C = 1$ nF (cell area = 0.1 mm²) and $G_L = 50$ nS is used for the passive membrane. The membrane equation is numerically integrated using the 4th-order Runge-Kutta method.

Booth-Rinzel-Kiehn Model

To verify our method in a more biophysically realistic model, we use the established Booth-Rinzel-Kiehn (BRK) model (Booth et al. 1997). The BRK model is a two-compartment (2C) model with intrinsic conductances representing the dynamics of vertebrate motor neurons, and therefore appropriate for our investigation. All the original published model parameters are also used in our study. The neuron is amended with time-varying G_e and G_i in the soma and dendritic compartment scaled with their respective surface fraction. The conductance time series are generated by adding Poisson-distributed α -synapses in the same way as in the GPS model (Eq. 16). Again, both τ_{syn} and g_{\max} are different for inhibition and excitation but otherwise constant for those inputs. Since the leak conductance ($g_{\text{leak}} = 0.51$ mS/cm²) in the BRK model is much larger than typical motoneurons [$g_{\text{leak}} \approx 0.05$ mS/cm² (Berg et al. 2008)], we use synaptic time constants that are much shorter ($\tau_{\text{syn},e} = 0.001$ ms and $\tau_{\text{syn},i} = 0.005$ ms) such that V dynamics is not dominated by their kinetics. For congruency between the GPS model and the original BRK model the conductance, current and capacitance are now in values per area. Thus the total synaptic conductances, i.e., somatic and dendritic conductances, are $g_{\max,e} = 17.8$ mS/cm² for excitation and $g_{\max,i} = 9.4$ mS/cm² for inhibition. The specific capacitance is set to 1 $\mu\text{F}/\text{cm}^2$, and current is in units of $\mu\text{A}/\text{cm}^2$. The balance of \bar{V} is achieved by adjusting the mean inhibitory conductance once given an excitatory conductance according to Eq. 17 in the somatic compartment. The synaptic input was distributed according to the size of the compartments (90% on dendrite 10% on soma) to get the same input rate per membrane area.

Data Simulation

The following reversal potentials are used in data simulations, $E_L = -70$ mV, $E_i = -80$ mV, and $E_e = 0$ mV. Since the sole purpose of the model is to investigate subthreshold fluctuations and membrane time constant the I and E input is balanced to enforce constant $\bar{V} = -60$ mV. An injected current is added to keep $\bar{V} = -60$ even during low intensity of synaptic input. Simulations are performed for time periods of 2 s (1 second in the BRK model) using time steps of 0.05 ms (0.005 ms in the BRK model) and analyzed with a data window size of 130 ms to be comparable with experimental data. All simulations are performed in Matlab (version R2011, Mathworks).

OU process. All OU processes are simulated using exact method (Gillespie 1996). In the simulation of V as an OU process we use the following parameters: $\tau = 1.3\text{--}40.3$ ms and $\sigma = 3$ V/s. In the simulations of the conductance-based model where synaptic conductance is modeled as two OU processes (the GOU model), the following parameters are used: respective for excitation and inhibition, time constants, and standard deviations are, $\tau_e = 0.5$ ms and $\tau_i = 1.0$ ms and $\sigma_e = 2\text{--}19$ nS/ $\sqrt{\text{ms}}$ ($SD_e = 1.0\text{--}9.5$ nS) and $\sigma_i = 2.7\text{--}23.9$ nS/ $\sqrt{\text{ms}}$ ($SD_i = 1.9\text{--}16.9$ nS), where the latter scale with the mean synaptic conductance.

Data Analysis and Software Package

All calculations were performed in Matlab. The custom-made procedures for estimating τ , C , G_{tot} , G_i , and G_e has been uploaded to mathworks code-sharing web site (<http://www.mathworks.com/matlabcentral/>) with the names “SynapticConductance” as a zipped folder for the interested reader. The software for estimating the effective recovery time (eRT) and synaptic integration time (eSIT) is called eRT.m to compare with τ to assess the contamination by spikes (Berg et al. 2008). The remaining Matlab code is available on request.

RESULTS

The present study introduces an approach to estimating the inhibitory and excitatory conductances. The method is based

on first estimating the total membrane conductance from τ in a time window for which stationarity is a valid approximation. This is accomplished by assuming that the electronic structure of the neuron can be approximated as one compartment and the major contributors to the total conductance are either synaptic and/or constant. Further, we have to assume stationarity in the window (Fig. 1).

Estimating Total Conductance: V as an OU Process

To verify the accuracy of estimating G_{tot} via the membrane time constant, we first look at a simulated OU process (Eq. 6), where the fluctuations are additive. The result of the simulation and estimation is summarized in Fig. 2. There is good agreement between input G_{tot} and the estimated both using MLE for the OU process and the ACF method, especially for higher conductance. The disparity between estimated and G_{tot} for lower values is due to the fact that the time constant is exceeding the data window size. The disparity also represents the observation that smaller conductance is generally harder to extract. The data window size is kept fixed for all simulations. Based on this analysis, we suggest that if V follows an OU process, the ACF method is comparable to the MLE and therefore a good estimator of G_{tot} .

Estimating Inhibition and Excitation in the Conductance-Based Models

The method of estimating the inhibition and excitation is first verified using two conductance-based models. First, the one-compartment model is where the synaptic conductance is modeled as two independent OU processes, one for inhibition and one for excitation. We refer to this model as the GOU model, since the conductance rather than the voltage is modeled as OU processes. The mean conductance is adjusted such that V is kept balanced. A GOU sample trace is shown (Fig. 3A). Second, the model with synaptic input is arriving as two independent Poisson processes, postsynaptically evoking α -function conductance, and where the rates of the input is adjusted to balance V , referred to as the GPS model. A sample trace is shown (Fig. 3B). The autocorrelation function of V in

both models has a decay, for which an exponential is fitted (Fig. 3C), and thus $G_{\text{tot}} = C/\tau$ is extracted (Fig. 3D). From G_{tot} , V , and Eqs. 3 and 4, the inhibition and excitation are estimated and in agreement with both the GOU-model input (Fig. 3E) and the GPS-model input (Fig. 3F).

Next, we analyze the more realistic two-compartment model including intrinsic properties called the BRK model (Booth et al. 1997) for further verification of our method (Fig. 4, A and B). Even when including random arrival of synaptic input as α -function conductances on both compartments, the V fluctuations still resembles those of the above models (Fig. 4C). Since the somato-dendritic distribution of synaptic contacts is unknown, we have analyzed three cases: 90, 50, and 10% of contacts on soma. For the two former cases, the estimates for the E and I conductances converge gracefully towards the synaptic input, i.e., the $x = y$ line, as the input intensity increases (dark and medium green and blue curves, Fig. 4D). In the latter case of 10% contacts on soma (light green and blue curves), the estimates are less precise, especially G_e , although they still have a monotonic increase with increasing input.

In this study, we utilize the analytical tractability of the OU process to establish the confidence levels of all estimates. Therefore, the accord between the MLE of the OU process (Fig. 2) and the ACF is important for the integrity of the analysis. The consensus between MLE and ACF is highly dependent on the choice of lag in the MLE (Fig. 3G). The dependence is due to ACF not having a purely monoexponential decay, as seen in the concave shape for small lags (Fig. 3C, inset). This effect is caused by V being more correlated with itself at small time lags than expected in an exponential decay, and this is mainly due to low-pass filtering of the synaptic processes. Since the MLE of OU processes uses a short lag to estimate G_{tot} , the MLE method is very sensitive to deviations from exponential decay at the origin. To remedy this effect, we increase the lag size, such that it is larger than these temporal microstructures. The MLE estimates approach stable values, somewhere in close proximity of the G_{tot} and the ACF estimate (Fig. 3G). This asymptotic approach suggests that there exist choices of lags in MLE for which the OU model is a valid description. This grants the reliability of the variance deduced

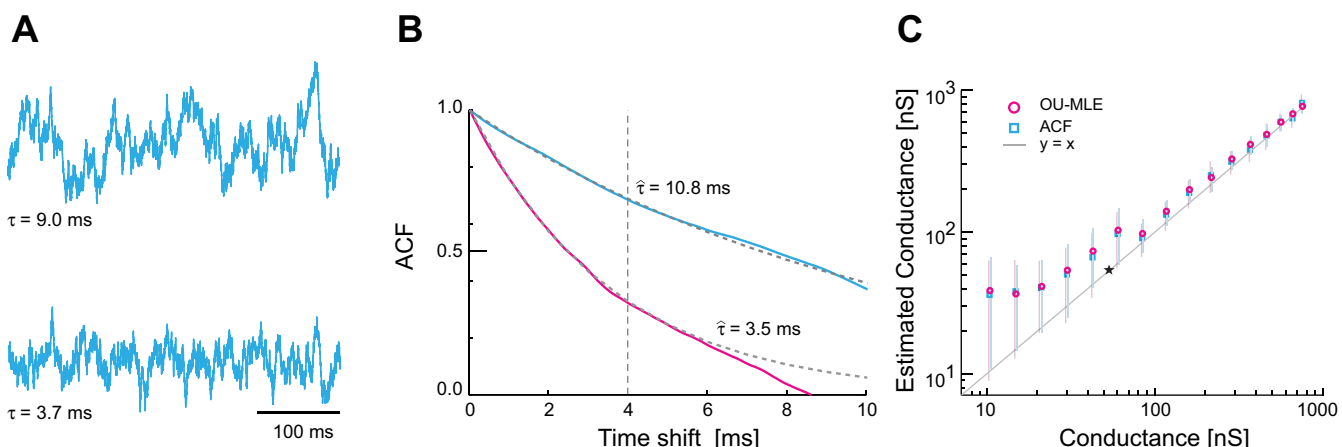


Fig. 2. Simulating membrane potential fluctuations as an Ornstein-Uhlenbeck (OU) process with different time constants. A: 2 traces with different G_{tot} and characteristic time constants (top trace: $\tau = 9.0$ ms; bottom trace: $\tau = 3.7$ ms). B: autocorrelation function (ACF) of the traces in A (cyan is the top trace and magenta is the bottom trace in A). Broken lines are the exp-fit from 0 to the vertical line. C: conductance in the OU model vs. the estimated values, maximum likelihood estimation in magenta and ACF method in cyan; the error bars are the trial-to-trial SD; $y = x$ is shown as a solid line. The point where τ is equal to the data window is indicated (\star).

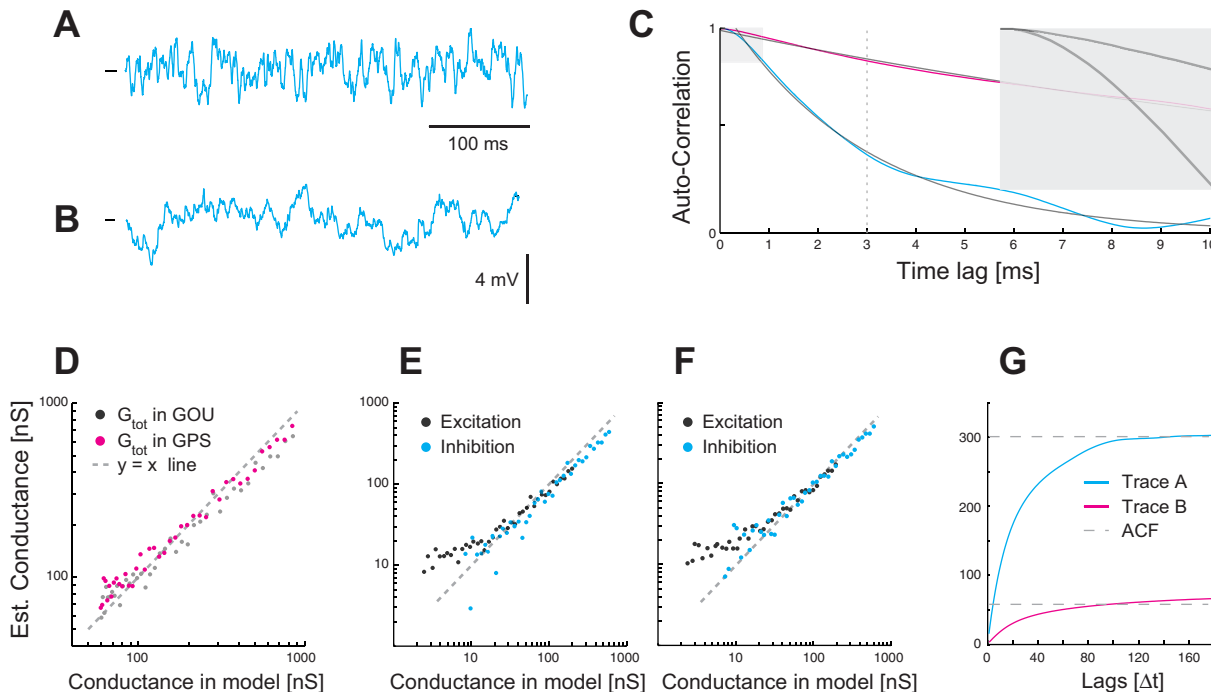


Fig. 3. Verification of G_{tot} and inhibition and excitation conductance (G_i , and G_e) estimation using data from 2 conductance models. Inhibition (I) and excitation (E) is modeled as 2 independent OU processes with different time constants (A; GOU model), variance, and mean ($G_e = 102$ nS and $G_i = 305$ nS) or 2 independent Poisson processes (B; GPS model) with rates adjusted to balance \bar{V} ($G_{tot} = 77.5$ nS, $G_e = 6.8$ nS, and $G_i = 20.5$ nS). C: ACF calculated from 130 ms of the sample traces in A (cyan) and B (magenta). The area close to the origin has concave curvature as shown in highlighted inset. D: total conductance vs. the estimated total conductance in both the GOU (dark) and the GPS model (magenta). E and F: estimated E and I vs. real conductance for different levels of input intensity for the GOU model (E) and the GPS model (F). Estimates of the sample trace in A is $G_e = 94$ nS and $G_i = 256$ nS. G: MLE of G_{tot} , assuming an OU process (solid line), converges towards the estimates using ACF (broken line) for larger lags. This is based on V data with same parameters as in A and C, except data window is 2 s.

from MLE of the OU process (Eqs. 9–11) and enables us to adopt the levels of confidence in other estimates, such as the ACF method. To test this assertion, we used both models to verify the estimates of G_{tot} , G_i , and G_e as well as their variance. The standard deviations of the estimates are in good agreement with the predicted both for G_{tot} (Fig. 5A) and G_i and G_e in the GOU model (Fig. 5B) and the GPS model (Fig. 5C). Notice that G_i has larger variance than G_e , and inhibition therefore represents the main contribution to the variance in G_{tot} .

Estimation on Real Data: Comparison Between Single and Multitrial Data

We use the ohmic estimate of G_{tot} (Fig. 6, A–C) to verify the accuracy of the ACF method in real data. Although the ohmic estimates have a source of error in both the conductance and the V estimates due to spikes (Guillamon et al. 2006), this has little or no effect on the conductance estimates. This is verified by plotting one conductance estimate vs. the other two and assess deviations from linearity. These plots have remarkable linearity (Fig. 6D). The weak effects of spikes are likely due to the intense synaptic input present in this particular network (Berg et al. 2008) causing the high-conductance state in the neuron and reducing the impact of intrinsic conductance (Berg and Hounsgaard 2009). We suggest that the ohmic estimate is a suitable comparison to evaluation of the ACF estimate.

Next, the V fluctuations are analyzed in data windows of 300 ms, providing estimates of G_{tot} as a function of time (Fig. 7A). This is performed by injecting a negative current to hyperpolarize the neurons and avoid spikes. The estimated G_{tot} using

ACF method is compared with the ohmic estimate and plotted with the 95%-confidence band around the estimate (Fig. 7B). The agreement between the ohmic and the ACF method is determined via their correlation (Fig. 7C) where 41% of the variation in G_{tot} can be explained by variation in the ohmic G_{tot} ($R = 0.64$). Although the correlation is contaminated by fluctuations for smaller choice of window sizes, it is robust over a wide range of window sizes (Fig. 7D, magenta.). The estimates of G_{tot} using MLE based on the OU process (denoted G_{MLE}) had a poor correlation with that based on the ACF method for small lags, but for lags around 20–30 Δt there was high correlation (Fig. 7D). This justifies using the variance estimates from the OU process as a surrogate variance in the ACF estimates. The ohmic estimates is subtracted from the estimates of G_{tot} and binned in a histogram to assess the limits of confidence in G_{tot} (Fig. 7E). The 95%-confidence limits only contained 79% of the data, so the variance in this case is underestimated. Part of this discrepancy is due to variance in the ohmic estimate. The mean conductance, however, has the center of mass close to zero (Fig. 7E), and there is therefore favorable agreement between the two estimates. The above analysis is done on other sets of trials with similar results (data not shown).

Estimating on Real Data: Pharmacology

As an additional means of verification, we modify inhibition and excitation via pharmacological manipulations in the experimental setup. The manipulation is applied locally via a small perfusion system that only touch the exposed spinal surface

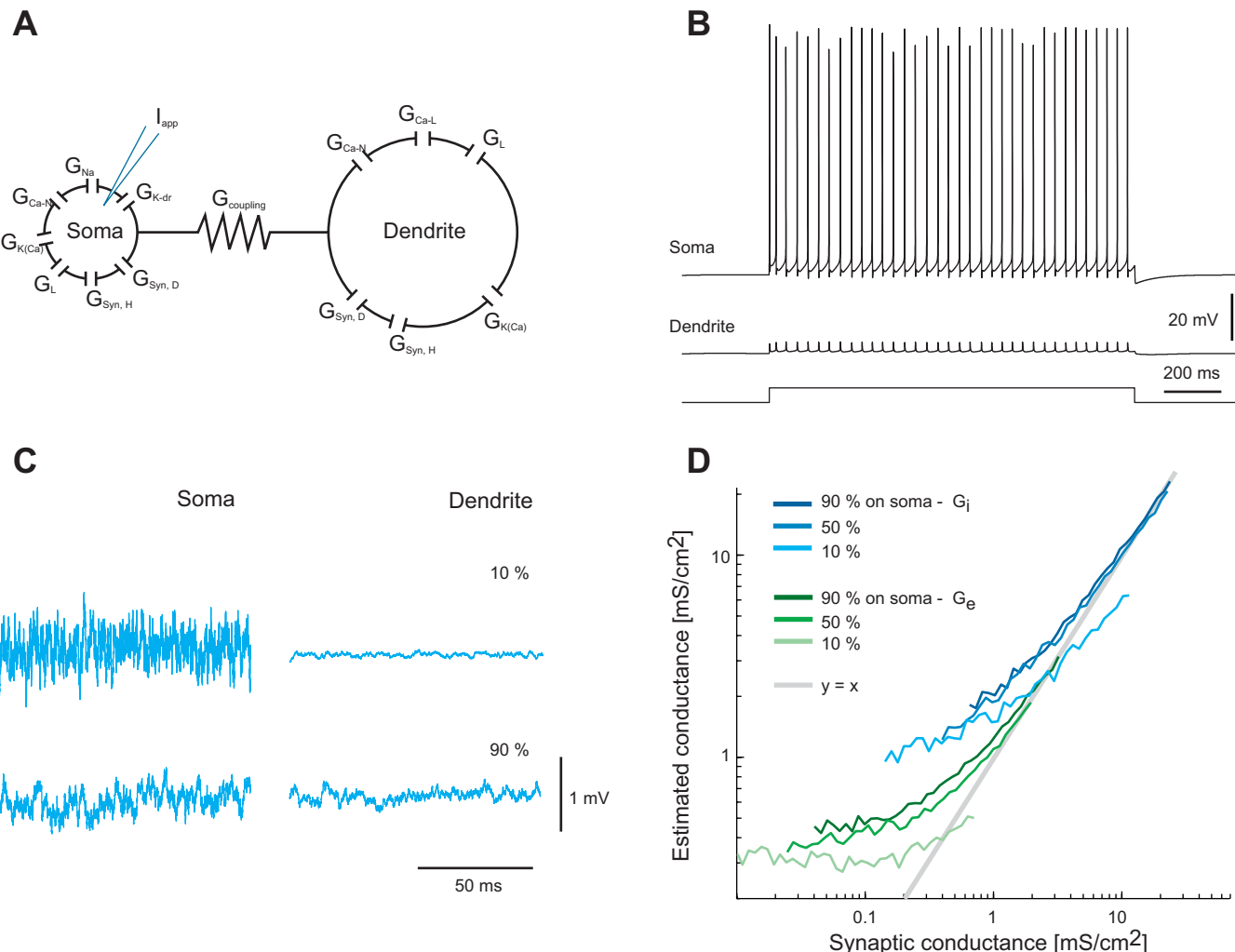


Fig. 4. Verification of method in 2-compartment model [Booth-Rinzel-Kiehn (BRK) model] containing multiple intrinsic conductances. *A*: schematics of the model. *B*: potential in soma (*top*) and dendrite (*middle*) given a constant somatic current injection ($I = 11 \mu\text{A}/\text{cm}^2$) similar to Fig 2B in Booth et al. (1997). *C*: sample traces of subthreshold membrane potential in soma (*left*) and in dendrite (*right*) with total synaptic conductance ($G_e = 0.4 \text{ mS}/\text{cm}^2$ and $G_i = 1.2 \text{ mS}/\text{cm}^2$) distributed 10% (*top*) and 90% (*bottom*) in the dendrite. *D*: estimated G_e (green) and G_i (blue) vs. synaptic conductance for different levels of input intensity and somato-dendritic distribution of synaptic contacts, all in subthreshold regime.

without affecting the rest of the network. First, we use the V recordings from spinal motoneurons receiving synaptic input during a motor program in a control condition. The nerve activity serves as monitor of the network state for identification of similar cycles in activity and to monitor constriction of pharmacology. G_{tot} , G_e , and G_i are then estimated in data windows of 300 ms in the control condition (Fig. 8A), after application of blocking of glycinergic inhibition with strychnine (Fig. 8B), and then finally adding the glutamatergic antagonist CNQX to the superfusion medium to block the main excitatory component (Fig. 8C). During the cycle, the inhibition (magenta) is largely zero after application of strychnine, which blocks glycine. This is also apparent since it is necessary to apply negative current to prevent the neuron from excessive spiking (Fig. 8B, *top middle trace*). Note that the synaptic fluctuations also change shape and are slower. Next, when the excitation is reduced pharmacologically, by addition of CNQX, the estimates are also reduced as expected and a positive current is necessary to induce a spike (Fig. 8C). Note how most

of the synaptic fluctuations are now abolished and the spike afterhyperpolarization is longer, since this intrinsic conductance is now strong enough to overcome the synaptic potential drive (Fig. 8C, *top trace*). The negative values of G_i is due to the variation of V being slower than the time constant, and G_{tot} is then smaller than G_{leak} (Fig. 8C, *middle bottom trace*).

To verify the levels of confidence in our estimates, the distributions of G_i , G_e , and G_{tot} are shown together with the predicted distributions as overlay (Fig. 9). The predicted distributions are based on (Eqs. 10–11), which provide the estimated statistical variances as they would occur from trial to trial. From single-trial experimental data, these variances cannot be extracted, but an approximation is obtained by the variance of the estimates over data windows, by assuming stationarity. Their widths show correlation and contain most of the data points (compare inhibition and excitation in the 3 conditions). Note that the excitation has the most narrow distribution and is therefore the most well determined. The largest contribution to total conductance comes from inhibition

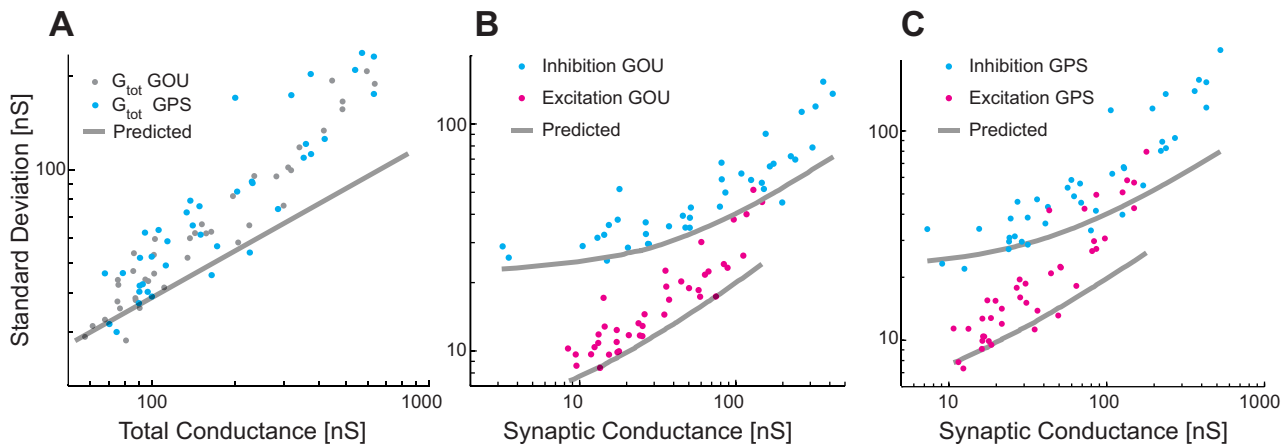


Fig. 5. SD of trial-to-trial conductance estimates compared with the predicted as a function of estimated conductance. A: SD of G_{tot} in 2 conductance-based models, the GOU model (gray points) and the GPS model (cyan points) compared with predicted (solid line, Eq. 9). B: SD of G_i (cyan) and G_e (magenta) estimates for the GOU model. Solid lines are the predicted from Eqs. 10 and 11. C: same as in B, but for GPS model.

(Fig. 9C), which is a consequence of the larger driving force for excitation. The uncertainty of the estimates (SD) is in remarkable agreement with the predicted (Fig. 9D).

DISCUSSION

In the present study we provide instruments to estimate the total conductance and inhibitory and excitatory synaptic con-

ductances on the basis of single-trial data. Furthermore, we provide confidence limits on the estimates of G_{tot} , G_i , and G_e (Eqs. 9–11). The confidence limits are independent of the particular choice of G_{tot} estimator. First, these estimates are verified in model data (Figs. 2–5), where the synaptic conductance is known. Second, estimates based on experiments are verified in data, where the synaptic conductance is either

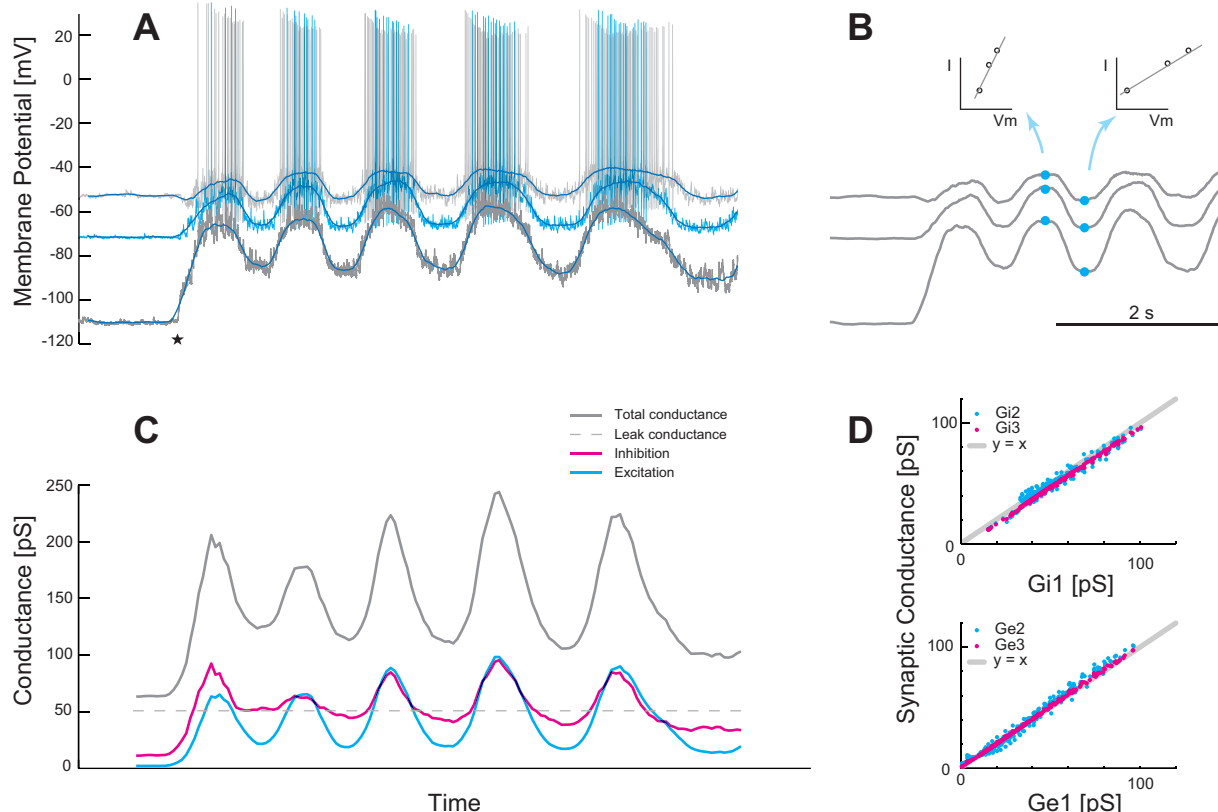


Fig. 6. Establishing control estimates of conductance using multiple trials and ohmic method. A: intracellular V recording in a motoneuron for 3 different current injections (top trace, +1.5 nA; middle trace, 0 nA; and bottom trace, -2.2 nA) with the low-pass filtered overlays. The motoneuron is part of a spinal network producing a scratch motor pattern in response to a tactile touch. The touch onset is indicated (\star). Note that the bottom trace has no spikes due to the hyperpolarizing current. B: low-pass filtered V from A as a function of time. I - V plots for locations on traces (indicated with the blue dots) and their slopes reveal G_{tot} as a function of time. C: G_{tot} as a function of time (gray line) with inhibitory (magenta) and excitatory (cyan) conductance estimated from Eqs. 3 and 4. Leak conductance is indicated with the broken line. D: 3 traces in A and B give 3 estimates of synaptic conductance. Each plotted against the other show remarkable linearity. Top: G_{i1} vs. G_{i2} (cyan) and G_{i3} (magenta). Bottom: G_{e1} vs. G_{e2} (cyan) and G_{e3} (magenta).

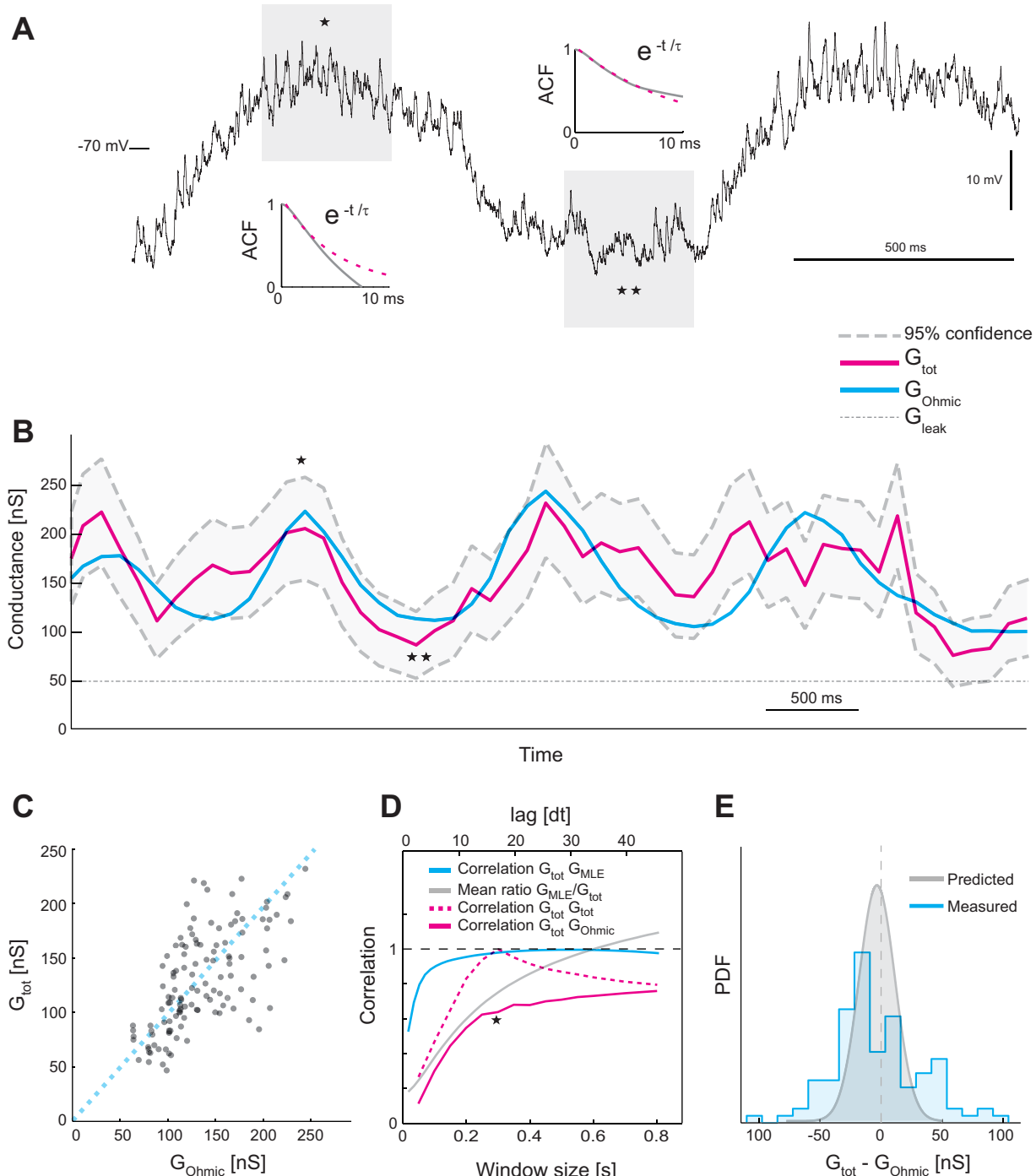


Fig. 7. Comparison between estimates of conductance. *A*: sample V recording in a motoneuron hyperpolarized to avoid spikes ($I_{\text{inj}} = -2.2 \text{ nA}$) with 2 regions highlighted. Statistics of the V fluctuations in the highlighted areas are calculated, shown is the autocorrelation function, which is fitted with exponential function decaying with τ . *B*: total ohmic conductance (from Fig. 6) plotted (cyan) with estimates based on ACF-decay (magenta) with 95% confidence limits (broken gray). The location of the sample windows are indicated for the depolarized (\star) and for the hyperpolarized ($\star\star$) window. *C*: ohmic G_{tot} is correlated with the conductance estimates using ACF-decay ($R = 0.64$; $P \ll 0.001$). *D*, top time base: correlation between G_{tot} from ACF and from MLE (G_{MLE}) for different sample point lags (cyan) and the ratio between the estimates (gray). Bottom time base: correlation between G_{tot} for window size of 300 ms and G_{tot} for different window sizes (broken magenta). Correlation between G_{tot} and the ohmic G_{tot} for different window sizes (magenta). The window size used in *B* and *C* is marked (\star). *E*: distribution of residuals of the two estimates (cyan) and the predicted variance in G_{tot} estimates (Eq. 9). This sample has 21% outside the 95% confidence limit.

compared with the ohmic method (Figs. 6–7) or manipulated pharmacologically (Figs. 8–9). Based on our results both from modeling and experimental verification, we suggest the method is reliable and provides a promising new tool for analyzing the network activity via intracellular recordings.

Levels of Confidence

The estimates of the variances of the estimators slightly underestimate the true variances (Figs. 5 and 7). This is probably due to the fact that these variances are the asymptotic variances obtained from the Fisher information, which are only

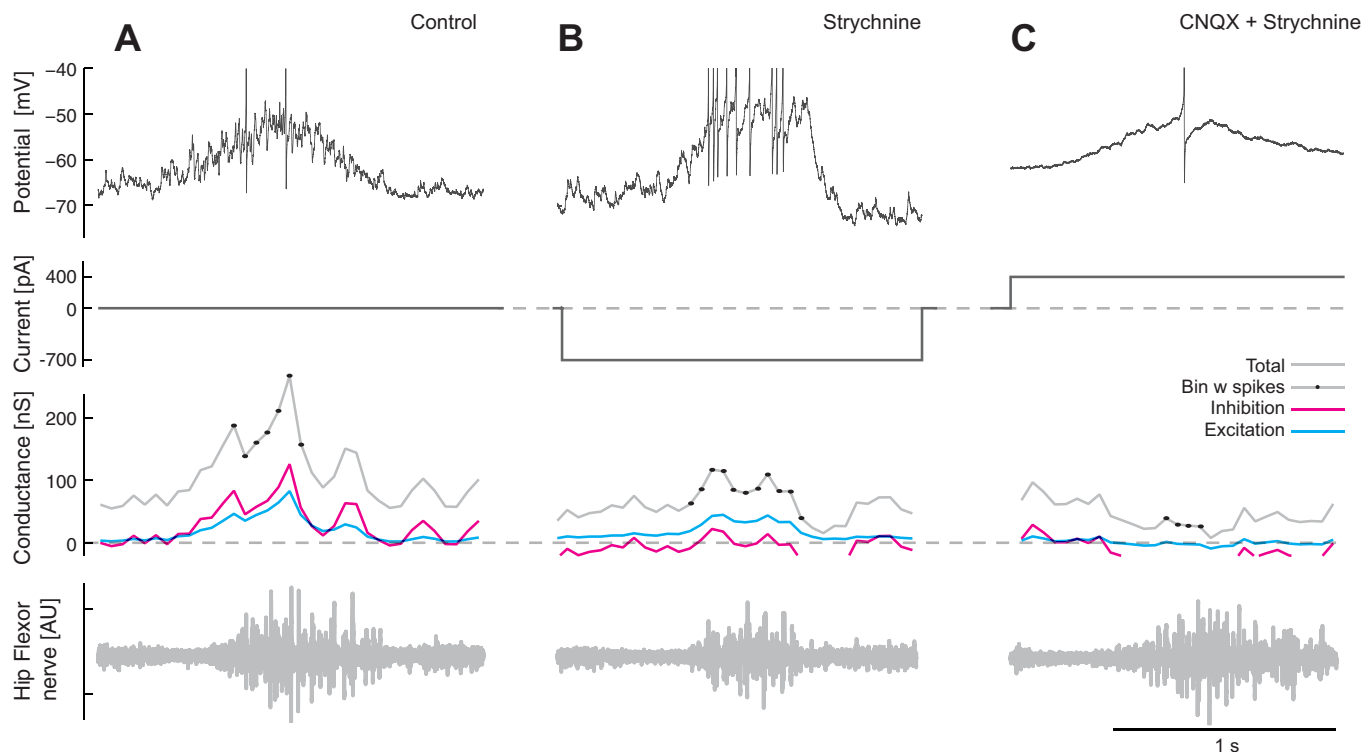


Fig. 8. Estimating conductance from V before and after pharmacological manipulation. **A:** control condition: recorded V for one scratch cycle (*top trace*) in current clamp ($I_{inj} = 0$, *top middle*). Estimated conductances (*bottom middle*) for 190-ms time windows (G_{tot} , gray), G_i (magenta), and G_e (cyan). Time windows containing spikes are indicated (●). The network state is indicated by the motor nerve activity at *bottom* (hip flexor). **B:** locally blocking inhibition by superfusion with strychnine results in larger depolarization in V (*top trace*) during the scratch cycle even when injecting negative current ($I_{inj} = -700$ pA, *top middle trace*). Both G_{tot} and G_i are reduced whereas G_e (cyan) and the network state (*bottom trace*) are largely unaffected. **C:** eliminating most excitation by addition of 6-cyano-7-nitroquinoxaline-2,3-dione (CNQX) to superfuse results in weak depolarization in V (*top trace*), which only spikes because of positive current injection ($I_{inj} = +400$ pA, *top middle trace*). Both G_i and G_e are now reduced (*bottom middle traces*), although the nerve activity remain largely unaffected (*bottom trace*). Spikes are clipped at -40 mV and conductance at -10 nS.

approximations to the variances in finite samples. In any case, these estimates are never far from the empirical variances and provide a useful tool for confidence evaluation. Furthermore, estimates of conductance based on MLE under the assumption of OU process converge towards the real values in the model (Fig. 3G) and in experiment (Fig. 7D), which suggests the levels of confidence provided in the present study can also be used in association with alternative measures such as the conventional method of multitrial ohmic method (Berg et al. 2007; Borg-Graham et al. 1998; Monier et al. 2008).

Conductance and Neuron Type

Both the leak and synaptic conductance of neurons used in this study are higher than those commonly observed in the forebrain. For instance, neocortical neurons in cats and ferrets sometimes have conductances an order of magnitude smaller (Haider et al. 2006; Ozeki et al. 2009). This is likely not due to difference in species but rather a difference in neuron size. The larger a neuron is, the more membrane area and leak currents contribute to the conductance. For instance, some of the largest neurons, found in the mammalian spinal cord, can easily be orders of magnitude larger than the neurons in the present study. The *gastrocnemius medialis* motor neurons typically have $G_{leak} \approx 300\text{--}600$ nS in rats and $G_{leak} \approx 500\text{--}1,700$ nS in cats (Kernell 2006) whereas the neurons used here have only $G_{leak} \approx 50$ nS. A larger neuron is likely to have more mem-

brane area devoted to synaptic contacts; and therefore, the synaptic conductance should also be larger. We expect that the synaptic conductance is appropriately adjusted with respect to the leak conductance to impact action potential generation. Therefore, the values of conductance in our sample neurons and model neurons should not be seen as a special case but rather seen as inspiration and for comparison. When comparing, the conductance values in Figs. 2–9 should be considered with respect to the leak and not their absolute values.

Regarding fitting time and window size adjustments in our method, these should be minor. A neuron of a larger morphology has larger conductance, but it will also have a proportionally larger capacitance. Therefore a difference in time constant ($\tau = C/G_{tot}$) cannot be attributed to a difference in the neuron size but rather due to a difference in membrane channel density, compartmentalization or membrane lipid dielectric constant. Using sharp electrodes one has to be aware of an additional shunt from tear in the membrane. This is typically a 50% increase in leak conductance compared with patch electrodes (Staley et al. 1992), and it is nonselective to any particular ion. As a consequence the synaptic conductance will be underestimated. Since the data presented in the present study are based on sharp electrodes, using whole cell patch recording, where the measured leak conductance is closer to the actual leak, is likely to improve the estimates of synaptic conductance.

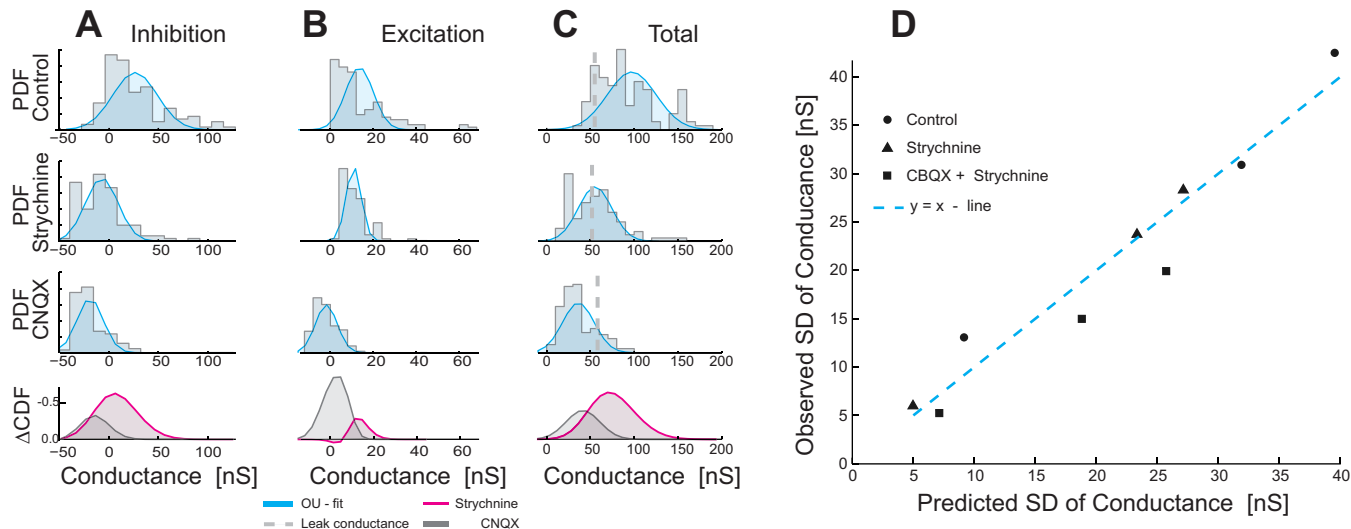


Fig. 9. Distribution of conductances before and after blockage of synaptic input with strychnine and CNQX. **A:** distribution of G_i in control condition (*top*), after application of strychnine (*top middle*) and after also blocking excitation (*bottom middle*). For comparison, the predicted Gaussian distribution (*Eqs. 10*) is superimposed (cyan). Largest pharmacological impact on G_i is the strychnine, as indicated by the difference in the cumulative distributions (*bottom*: strychnine: magenta; CNQX: gray). **B:** distribution of G_e is largely unaffected after application of strychnine (compare *top* and *top middle*), whereas it is close to zero after CNQX (*bottom middle*). The superimposed Gaussian curve is the predicted (*Eq. 11*). This is expressed in the cumulatives that have the largest difference before and after CNQX (gray) and smallest after strychnine (magenta). **C:** largest effect of pharmacology on the distribution of G_{tot} is strychnine (compare *top* with *top* and *bottom middle*), which is also indicated in the differences in the cumulatives (strychnine: magenta; CNQX: gray). Time windows containing spikes are not included in the estimates. **D:** predicted SDs of the conductance (*Eqs. 9–11*) vs. the measured with significant correlation ($R = 0.97$; $P \ll 0.001$). The smallest, middle, and largest values of the 3 cases are the SD of G_e , G_i , and G_{tot} , respectively.

Gap Junction Coupling

Gap junctions that embark upon the neuron are similar to injecting unknown currents of unknown dynamics. It is difficult to measure gap-junction currents because they depend on the preneuron activity. For this reason, gap junctions represent a source of error in estimating the synaptic conductance. A way to verify gap-junction coupling is to apply a tracer Neurobiotin (Vector Laboratories, Burlingame, CA) in the electrode pipette, since it crosses most types of gap-junctions, and then perform a histological examination (Bautista et al. 2012; Berkowitz et al. 2006). Similarly, immunofluorescent labeling with Lucifer yellow for instance can identify the connexins constituting the gap junctions. For a general review on tracers see Abbaci et al. (2008). Nevertheless, a more direct verification is via electrophysiology: if V depolarizes or hyperpolarizes in the course of the experiment without a change in G_{tot} , the depolarization/hyperpolarization is probably due to gap-junction currents, especially if $G_{tot} \approx G_L$. Generally, the higher the conductance change is (preferably at least $>50\%$ of G_{leak}), the more valid the ohmic assumption and the synaptic estimates are (*Eqs. 2, 3, and 4*). Additionally, smaller synaptic conductance is harder to differentiate (Figs. 2 and 3). Since the presence of gap-junction coupling is more ubiquitous in the developing nervous system where it is likely to serve a role in biochemical signaling (Chang et al. 1999) and in shaping of the circuitry (Personius et al. 2007), one should exercise caution using the present methods. For instance, the gap junction coupling in the neonatal rat spinal cord is strong enough that fictive locomotor activity induced by pharmacology [*N*-methyl-D-aspartate (NMDA) and 5-hydroxytryptamine (5-HT)] is present even without action potentials (Tresch and Kiehn 2000). Nevertheless, the ohmic method was recently applied on neonatal mouse spinal cord experiments to investigate the E/I-

synaptic dynamics during fictive locomotion (Endo and Kiehn 2008). It is difficult to interpret data from such experiments for three reasons. First, much of the dynamics are likely to involve current through electrical couplings. Second, the conductance is low and constant, especially in the flexor motoneurons ($\Delta G_{tot} < 10\%$), in spite of the substantial change in V (Endo and Kiehn 2008). Third, although they did not find any nonlinearities, neurons are chronically exposed to neuromodulators (NMDA/5-HT) that enhance intrinsic properties, which are generally difficult to account for. A way to incorporate these enhanced intrinsic properties would be to investigate their voltage dependence in the isolated neuron and then apply *Eqs. 13* and *14* (see MATERIALS AND METHODS). For these reasons, the methods generally apply better in neural systems that exhibit high-conductance states (Destexhe et al. 2003; Alaburda et al. 2005) generated from within the network dynamics as opposed to from pharmacological activation of intrinsic conductance. The method works better when the synaptic conductance is higher, since this underpins the assumptions, we therefore suggest the estimates of G_{tot} should be at least twice as big as G_{leak} .

Spike Contamination

The presence of action potentials in the V trace is likely to bias the E/I estimates. Therefore, it is preferred to force V into the subthreshold regime, e.g., via negative current injection, to improve the estimates. Nevertheless, if spikes are present, we recommend using a smaller sliding window for estimation at the cost of higher variance (*Eqs. 9–11*) and then excluding the windows containing spikes.

For assessing how long a spike has an impact on V , we suggest using the statistical approach introduced by Berg et al. (2008) of comparing the distribution of spike triggered overlay of V -trajectories before and after a spike with a template

distribution. This method provides a means to assess the impact of the transiently evoked intrinsic conductance associated with the spike. The temporal metrics in this method is called the effective synaptic integration time (eSIT) and the effective recovery time (eRT). The eSIT is defined as the time it takes to sum up enough synaptic input to cause a spike. The eRT is defined as the time it takes for the V distribution following a spike to return to the prespike condition, i.e., how long it takes the cell to forget that a spike has occurred (Berg et al. 2008). Since both the eRT and the eSIT were approximately equal to the τ during high-intensity synaptic input, the error in removing the spike from eSIT before the spike until eRT after the spike will be minimal. It was also found that the spike-evoked afterhyperpolarization was absent after the eRT. Therefore, if the window of removal around the spike is larger than eRT after the spike and eSIT before the spike, the increase in intrinsic conductance should be negligible.

Push-Pull vs. Balanced E/I

The situation of inhibition not arriving in concurrence with excitation, but rather in alternation with excitation, is referred to as *push-pull* input. Push-pull arrangements are well-documented in simple reflex systems, for instance, proprioceptive spinal feedback (Johnson et al. 2012). The push-pull input is relatively easy to distinguish from the balanced E/I input, since the G_{tot} is relatively constant in time in the push-pull. In the balanced input, G_{tot} increases considerably compared with the degree of depolarization (Berg and Hounsgaard 2009). In balanced E/I, one would see a weak increase in the spiking during depolarization, whereas the conductance increase severalfold compared with G_L . Thus the functional benefit of balanced E/I could be to expand the dynamic range of the input-output properties of the neuron (Baca et al. 2008; Saywell and Feldman 2004) either via increasing the V fluctuation (Chance et al. 2002; Destexhe et al. 2003) or by shifting the active region of a nonlinear IO-function (Silver 2010).

Summary of Requirements

The time constants of EPSCs and IPSCs have to be shorter than the passive membrane time constant; otherwise, the ACF method will underestimate the synaptic conductance. It is therefore recommended to consider the synaptic time constants and compare them to the membrane time constant found via the ACF method. If they are comparable, E/I will be underestimated. A contrasting situation is if there are spikes or other time-dependent intrinsic conductances present, which will tend to overestimate E/I. It is therefore recommended to minimize the number of spikes in the V trace if possible. The presence of gap junctions can distort the E/I estimates in both directions, and it is recommended to assess how dominant they are in controlling V and possibly conduct histological controls. Finally, it is essential that synaptic input is present in considerable amount. If only low-intensity input is present, such that single EPSPs or IPSPs are clearly visible and separated, the ACF method is likely to measure the time constant of the electronic noise, which is much faster than the passive membrane time constant distorting the estimates upwards. Therefore, one should be cautious if the conductance estimate is high during low-intensity input and possible verify this via e.g., current pulse injections.

ACKNOWLEDGMENTS

We thank Mikkel Vestergaard and Peter Petersen for comments on an early version of the manuscript. The work is part of the Dynamical Systems Interdisciplinary Network, University of Copenhagen.

GRANTS

Funding was provided by Novonordic Foundation (to R. W. Berg), Danish Council for Independent Research—Medical Sciences (to R. W. Berg), and Danish Council for Independent Research—Natural Sciences (to S. Ditlevsen).

AUTHOR CONTRIBUTIONS

Author contributions: R.W.B. and S.D. conception and design of research; R.W.B. performed experiments; R.W.B. analyzed data; R.W.B. and S.D. interpreted results of experiments; R.W.B. prepared figures; R.W.B. and S.D. drafted manuscript; R.W.B. and S.D. edited and revised manuscript; R.W.B. and S.D. approved final version of manuscript.

REFERENCES

- Abbaci M, Barberi-Heyob M, Blondel W, Guillemin F, Didelon J. Advantages and limitations of commonly used methods to assay the molecular permeability of gap junctional intercellular communication. *Biotechniques* 45: 33–52, 56–62, 2008.
- Alaburda A, Hounsgaard J. Metabotropic modulation of motoneurons by scratch-like spinal network activity. *J Neurosci* 23: 8625–8629, 2003.
- Alaburda A, Russo R, MacAulay N, Hounsgaard J. Periodic high-conductance states in spinal neurons during scratch-like network activity in adult turtles. *J Neurosci* 25: 6316–6321, 2005.
- Azouz R, Gray CM. Cellular mechanisms contributing to response variability of cortical neurons in vivo. *J Neurosci* 19: 2209–2223, 1999.
- Baca SM, Marin-Burgin A, Wagenaar AD, Kristan WB. Widespread inhibition proportional to excitation controls the gain of a leech behavioral circuit. *Neuron* 57: 276–289, 2008.
- Bachar M, Batzel J, Ditlevsen S. (Editors) Stochastic biomathematical models with applications to neuronal modeling. In: *Lecture Notes in Mathematics, Mathematical Biosciences Subseries*. New York: Springer, vol. 2058, 2013.
- Bartlett MS. On the theoretical specification and sampling properties of autocorrelated time-series. *Suppl J Royal Stat Soc* 8: 27–41, 1946.
- Bautista W, Nagy JI, Dai Y, McCrea DA. Requirement of neuronal connexin36 in pathways mediating presynaptic inhibition of primary afferents in functionally mature mouse spinal cord. *J Physiol* 16: 3821–3839, 2012.
- Berg RW, Hounsgaard J. Signaling in large-scale neural networks. *Cogn Proc* 10, Suppl 1: S9–15, 2009.
- Berg RW, Alaburda A, Hounsgaard J. Balanced inhibition and excitation drive spike activity in spinal half-centers. *Science* 315: 390–393, 2007.
- Berg RW, Ditlevsen S, Hounsgaard J. Intense synaptic activity enhances temporal resolution in spinal motoneurons. *PLoS One* 3: e3218, 2008.
- Berkowitz A, Yosten GL, Ballard RM. Somato-dendritic morphology predicts physiology for neurons that contribute to several kinds of limb movements. *J Neurophysiol* 95: 2821–2831, 2006.
- Bibbona E, Ditlevsen S. Estimation in discretely observed Markov processes killed at a threshold. *Scand J Stat* 40: 274–293, 2013.
- Booth V, Rinzel J, Kiehn O. Compartmental model of vertebrate motoneurons for Ca^{2+} -dependent spiking and plateau potentials under pharmacological treatment. *J Neurophysiol* 78: 3371–3385, 1997.
- Borg-Graham LJ, Monier C, Frégnac Y. Visual input evokes transient and strong shunting inhibition in visual cortical neurons. *Nature* 393: 369–373, 1998.
- Chance FS, Abbott LF, Reyes AD. Gain modulation from background synaptic input. *Neuron* 35: 773–782, 2002.
- Chang Q, Gonzalez M, Pinter MJ, Balice-Gordon RJ. Gap junctional coupling and patterns of connexin expression among neonatal rat lumbar spinal motor neurons. *J Neurosci* 19: 10813–10828, 1999.
- Cobos I, Calcagnotto ME, Vilaythong AJ, Thwin MT, Noebels JL, Baraban SC, Rubenstein JL. Mice lacking Dlx1 show subtype-specific loss of interneurons, reduced inhibition and epilepsy. *Nat Neurosci* 8: 1059–1068, 2005.
- de Almeida AT, Kirkwood PA. Multiple phases of excitation and inhibition in central respiratory drive potentials of thoracic motoneurons in the rat. *J Physiol* 588: 2731–2744, 2010.

- Destexhe A, Paré D.** Impact of network activity on the integrative properties of neocortical pyramidal neurons in vivo. *J Neurophysiol* 81: 1531–1547, 1999.
- Destexhe A, Rudolph M, Paré D.** The high-conductance state of neocortical neurons in vivo. *Nat Rev Neurosci* 4: 739–751, 2003.
- Dichter M, Ayala G.** Cellular mechanisms of epilepsy: a status report. *Science* 237: 157–164, 1987.
- Ditlevsen S, Lansky P.** Estimation of the input parameters in the Ornstein-Uhlenbeck neuronal model. *Phys Rev E* 71: 011907, 2005.
- Ditlevsen S, Lansky P.** Only through perturbation can relaxation times be estimated. *Phys Rev E* 86: 050102(R), 2012.
- Endo T, Kiehn O.** Asymmetric operation of the locomotor central pattern generator in the neonatal mouse spinal cord. *J Neurophysiol* 100: 3043–3054, 2008.
- Forman JL, Sørensen M.** The Pearson diffusions: a class of statistically tractable diffusion processes. *Scand J Stat* 35: 438–465, 2008.
- Gerstner W, Kistler WM.** *Spiking Neuron Models*. Cambridge, UK: Cambridge Univ. Press, 2002.
- Gillespie D.** Exact numerical simulation of the Ornstein-Uhlenbeck process and its integral. *Phys Rev E Stat Phys Plasmas Fluids Relat Interdiscip Topics* 54: 2084–2091, 1996.
- Golowasch J, Thomas G, Taylor A.** Membrane capacitance measurements revisited: dependence of capacitance value on measurement method in nonisopotential neurons. *J Neurophysiol* 102: 2161–2175, 2009.
- Guillamon A, McLaughlin DW, Rinzel J.** Estimation of synaptic conductances. *J Physiol (Paris)* 100: 31–42, 2006.
- Haider B, Duque A, Hasenstaub AR, McCormick AD.** Neocortical network activity in vivo is generated through a dynamic balance of excitation and inhibition. *J Neurosci* 26: 4535–4545, 2006.
- Hasenstaub A, Sachdev RN, McCormick AD.** State changes rapidly modulate cortical neuronal responsiveness. *J Neurosci* 27: 9607–9622, 2007.
- Hastie T, Tibshirani R, Friedman J.** *The Elements of Statistical Learning* (2nd ed.). New York: Springer-Verlag, 2008.
- Jahn P, Berg RW, Hounsgaard J, Ditlevsen S.** Motoneuron membrane potentials follow a time inhomogeneous jump diffusion process. *J Comput Neurosci* 31: 563–579, 2011.
- Johnson MD, Hyngstrom AS, Manuel M, Heckman CJ.** Push-pull control of motor output. *J Neurosci* 32: 4592–4599, 2012.
- Kehler C, Maziashvili N, Dugladze T, Gloveli T.** Altered excitatory-inhibitory balance in the NMDA-hypofunction model of schizophrenia. *Front Mol Neurosci* 1: 1–7, 2008.
- Kendall M.** *Time-Series* (2nd ed.). London, UK: Charles Griffin, 1976.
- Kernell D.** *The Motoneurone and Its Muscle Fibres*. New York: Oxford Univ. Press, 2006.
- Kobayashi R, Shinomoto S, Lansky P.** Estimation of time-dependent input from neuronal membrane potential. *Neural Comput* 23: 3070–3093, 2011.
- Kolind J, Hounsgaard J, Berg RW.** Opposing effects of intrinsic conductance and correlated synaptic input on V_m -fluctuations during network activity. *Front Comput Neurosci* 6: 40, 2012.
- Kuhn A, Aertsen A, Rotter S.** Neuronal integration of synaptic input in the fluctuation-driven regime. *J Neurosci* 24: 2345–2356, 2004.
- Maltenfort MG, Phillips CA, McCurdy ML, Hamm TM.** Determination of the location and magnitude of synaptic conductance changes in spinal motoneurons by impedance measurements. *J Neurophysiol* 92: 1400–1416, 2004.
- Mariño J, Schummers J, Lyon DC, Schwabe L, Beck O, Wiesing P, Obermayer K, Sur M.** Invariant computations in local cortical networks with balanced excitation and inhibition. *Nat Neurosci* 8: 194–201, 2005.
- Monier C, Fournier J, Frégnac Y.** In vitro and in vivo measures of evoked excitatory and inhibitory conductance dynamics in sensory cortices. *J Neurosci Methods* 169: 323–365, 2008.
- Okun M, Lampl I.** Instantaneous correlation of excitation and inhibition during ongoing and sensory-evoked activities. *Nat Neurosci* 11: 535–537, 2008.
- Ozeki H, Finn IM, Schaffer ES, Miller KD, Ferster D.** Inhibitory stabilization of the cortical network underlies visual surround suppression. *Neuron* 62: 578–592, 2009.
- Palop JJ, Chin J, Mucke L.** A network dysfunction perspective on neurodegenerative diseases. *Nature* 443: 768–773, 2006.
- Parkis AM, Dong X, Feldman JL, Funk GD.** Concurrent inhibition and excitation of phrenic motoneurons during inspiration: phase-specific control of excitability. *J Neurosci* 19: 2368–2380, 1999.
- Pavliotis GA, Stuart AM.** Parameter estimation for multiscale diffusions. *J Stat Phys* 127: 741–781, 2007.
- Personius KE, Chang Q, Mentis GZ, O'Donovan MJ, Balice-Gordon RJ.** Reduced gap junctional coupling leads to uncorrelated motor neuron firing and precocious neuromuscular synapse elimination. *Proc Natl Acad Sci USA* 104: 11808–11813, 2007.
- Pospischil M, Piwkowska Z, Bal T, Destexhe A.** Extracting synaptic conductances from single membrane potential traces. *Neuroscience* 158: 545–552, 2009.
- Roberson ED, Halabisky B, Yoo JW, Yao J, Chin J, Yan F, Wu T, Hamto P, Devidze N, Yu GQ, Palop JJ, Noebels JL, Mucke L.** Amyloid- β /Fyn-induced synaptic, network, and cognitive impairments depend on tau levels in multiple mouse models of Alzheimer's disease. *J Neurosci* 31: 700–711, 2011.
- Rudolph M, Piwkowska Z, Badoual M, Bal T, Destexhe A.** A method to estimate synaptic conductances from membrane potential fluctuations. *J Neurophysiol* 91: 2884–2896, 2004.
- Russo RE, Hounsgaard J.** Dynamics of intrinsic electrophysiological properties in spinal cord neurones. *Prog Biophys Mol Biol* 72: 329–365, 1999.
- Sasaki K, Brezina V, Weiss KR, Jing J.** Distinct inhibitory neurons exert temporally specific control over activity of a motoneuron receiving concurrent excitation and inhibition. *J Neurosci* 29: 11732–11744, 2009.
- Saywell SA, Feldman JL.** Dynamic interactions of excitatory and inhibitory inputs in hypoglossal motoneurons: respiratory phasing and modulation by PKA. *J Physiol* 554: 879–889, 2004.
- Shadlen MN, Newsome WT.** Noise, neural codes and cortical organization. *Curr Opin Neurobiol* 4: 569–579, 1994.
- Shu, Y, Hasenstaub A, McCormick DA.** Turning on and off recurrent balanced cortical activity. *Nature* 423: 288–293, 2003.
- Silver RA.** Neuronal arithmetic. *Nat Rev Neurosci* 11: 474–489, 2010.
- Staley KJ, Otis TS, Mody I.** Membrane properties of dentate gyrus granule cells: comparison of sharp microelectrode and whole-cell recordings. *J Neurophysiol* 67: 1346–1358, 1992.
- Tresch MC, Kiehn O.** Motor coordination without action potentials in the mammalian spinal cord. *Nat Neurosci* 3: 593–599, 2000.
- Tuckwell HC.** Introduction to theoretical neurobiology. *Nonlinear and Stochastic Theories*. Cambridge, UK: Cambridge Univ. Press vol. 2, 1988.
- van Vreeswijk C, Sompolinsky H.** Chaos in neuronal networks with balanced excitatory and inhibitory activity. *Science* 274: 1724–1726, 1996.
- Wehr M, Zador AM.** Balanced inhibition underlies tuning and sharpens spike timing in auditory cortex. *Nature* 426: 442–446, 2003.
- Wilent WB, Contreras D.** Synaptic responses to whisker deflections in rat barrel cortex as a function of cortical layer and stimulus intensity. *J Neurosci* 24: 3985–3998, 2004.
- Yarom Y, Hounsgaard J.** Voltage fluctuations in neurons: signal or noise? *Physiol Rev* 91: 917–929, 2011.